

***Ab initio* study of charge transfer in B^{2+} low-energy collisions with atomic hydrogen**

A. R. Turner* and D. L. Cooper†

Department of Chemistry, University of Liverpool, Liverpool L69 7ZD, United Kingdom

J. G. Wang‡ and P. C. Stancil§

Department of Physics and Astronomy and the Center for Simulational Physics, The University of Georgia, Athens, Georgia 30602-2451, USA

(Received 3 September 2002; published 9 July 2003)

Charge transfer processes due to collisions of ground state $B^{2+}(2s^2S)$ ions with atomic hydrogen are investigated using the quantum-mechanical molecular-orbital close-coupling (MOCC) method. The MOCC calculations utilize *ab initio* adiabatic potentials and nonadiabatic radial and rotational coupling matrix elements obtained with the spin-coupled valence-bond approach. Total and state-selective cross sections and rate coefficients are presented. Comparison with the existing experiments shows our results to be in good agreement. When $E < 80$ eV/u, the differences between the current total MOCC cross sections with and without rotational coupling are small ($< 3\%$). Rotational coupling becomes more important with increasing energy: for collision energies $E > 400$ eV/u, inclusion of rotational coupling increases the total cross section by 50%–80%, improving the agreement between the current calculations and experiments. For state-selective cross sections, rotational coupling induces mixing between different symmetries; however, its effect, especially at low collision energies, is not as important as had been suggested in previous work.

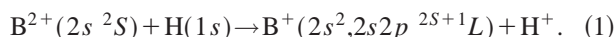
DOI: 10.1103/PhysRevA.68.012704

PACS number(s): 34.50.-s, 34.20.Mq, 34.70.+e

I. INTRODUCTION

Electron capture, or charge exchange, is an important atomic collision process in astrophysical and laboratory environments. It can influence the plasma ionization balance and the ion emission spectrum by populating excited states. This spectrum can also be used as a tool to diagnose plasma properties. In controlled thermonuclear fusion research, the walls of most plasma fusion devices are coated with boron. Due to erosion of the wall, a number of boron impurities will appear at the edge of the plasma. The charge transfer processes between boron impurities and H or He beams will play important roles in the plasma ionization balance and the ion emission spectrum.

In this paper, we study the charge transfer processes



Experimentally, total single electron capture (SEC) cross sections for this system have been measured using an electrostatic deflection method, with a tungsten furnace generating the atomic hydrogen, by McCullough *et al.* [1] (0.8 to 40 keV) and by Goffe *et al.* [2] (100 to 2500 keV). Crandall *et al.* [3] (10 to 30 keV) and Gardner *et al.* [4] (12 to 46 keV) used an electrostatic deflection method but with a standard H_2 gas cell heated to 2350 and 2500 K, respectively, to generate the hydrogen atoms. The cross sections of Mc-

Cullough *et al.* [1], of Crandall *et al.* [3] and of Gardner *et al.* [4] agree closely over all the coincident energy values.

This system has been studied theoretically by Crothers and Todd [5] using the phase integral of the two-state exponential model within the impact parameter formulation. They calculated the total SEC cross section but only considered capture to $B^+(2s^2^1S)$. Their calculated cross sections are in disagreement with the experimental data. This is probably due to the fact that only one SEC channel was treated. A more recent theoretical study by Honvault *et al.* [6] considered SEC to additional $1,3\Sigma^+$ and $1,3\Pi$ states between 0.1 and 190 keV. The adiabatic potentials and nonadiabatic radial and rotational coupling were computed using the CIPSI [7] configuration interaction (CI) method. Those adiabatic potentials and nonadiabatic coupling were then used to calculate total and state-selective cross sections via a semiclassical scattering formalism. Their total cross sections reproduce the experimental results much better than did the earlier study of Crothers and Todd [5].

In this work the quantum-mechanical molecular-orbital close-coupling (MOCC) method is used. The MOCC calculations utilize *ab initio* adiabatic potentials and nonadiabatic radial and rotational coupling matrix elements obtained with the spin-coupled valence-bond approach. Total and state-selective cross sections are calculated and compared with the available theoretical and experimental results. Total and state-selective rate coefficients are also presented. Section II describes the molecular potential and coupling data utilized in the MOCC calculations, while Sec. III discusses the scattering calculation approach. Section IV presents the results of the scattering calculation including comparisons of total and state-selective cross sections with other theories and experiments, while Sec. V briefly gives a summary of the work. Atomic units are used throughout unless otherwise noted.

*Present address: Department of Chemistry, University of Edinburgh, West Mains Road, Edinburgh EH9 3JJ, U.K. Electronic address: Andrew.Turner@ed.ac.uk

†Electronic address: dlc@liv.ac.uk

‡Electronic address: wangjg@physast.uga.edu

§Electronic address: stancil@physast.uga.edu

TABLE I. Asymptotic separated-atom energies for the states of $[\text{BH}]^{2+}$.

Molecular states	Asymptotic atomic states	Energy (eV)	
		Theory ^a	Expt ^b
1 $^1\Sigma^+$	$\text{B}^+(2s^2\ ^1S) + \text{H}^+$	-11.76	-11.56
1 $^3\Sigma^+$	$\text{B}^+(2s2p\ ^3P^o) + \text{H}^+$	-6.96	-6.93
1 $^3\Pi$	$\text{B}^+(2s2p\ ^3P^o) + \text{H}^+$	-6.95	-6.93
2 $^1\Sigma^+$	$\text{B}^+(2s2p\ ^1P^o) + \text{H}^+$	-2.21	-2.46
1 $^1\Pi$	$\text{B}^+(2s2p\ ^1P^o) + \text{H}^+$	-2.23	-2.46
3 $^1\Sigma^+$	$\text{B}^{2+}(2s\ ^2S) + \text{H}(1s^2S)$	0.0	0.0
2 $^3\Sigma^+$	$\text{B}^{2+}(2s\ ^2S) + \text{H}(1s^2S)$	0.0	0.0

^aThis work.^bNIST Atomic Spectra Database, 1999.

II. ELECTRONIC STRUCTURE CALCULATIONS

The adiabatic potential energy curves, nonadiabatic radial coupling, and rotational coupling for the four symmetries of interest ($^1\Sigma^+$, $^1\Pi$, $^3\Sigma^+$, and $^3\Pi$) were obtained using the spin-coupled valence-bond (SCVB) method (see, for example, Cooper *et al.* [8]). This is a fully flexible *ab initio* technique and, as such, we expect the molecular region to be described with much the same accuracy as the asymptotic separated-atom limit.

A Gaussian basis set of TZVP (triple zeta valence polarization) quality (taken directly from the GAMESS-UK package [9] and tabulated by Turner [10]) was used to describe both boron and hydrogen. As the boron core electrons ($1s^2$) were assumed to have little or no influence on the charge transfer process they were described using natural orbitals taken from a singlet multiconfigurational self-consistent field (MCSCF) calculation from within MOLPRO [11] and were not relaxed in the SC calculation. The remaining two valence electrons were accommodated in fully optimized, nonorthogonal spin-coupled orbitals within a SC calculation to give either a $^1\Sigma^+\text{B}^+(2s^2) + \text{H}^+$ configuration (for $^1\Sigma^+$ states), a $^3\Sigma^+\text{B}^+(2s2p\ ^3P) + \text{H}^+$ configuration (for $^3\Sigma^+$ states), or a $^1,3\Sigma^-\text{B}^+(2p^2) + \text{H}^+$ configuration (for $^1\Pi$ and $^3\Pi$ states, respectively).

Separate virtual orbital selections and SCVB (nonorthogonal CI) expansions were then generated for each of the four molecular symmetries of interest. The SCVB configuration space for each case was constructed by performing all single and double vertical excitations, along with singly ionic excitations, that yielded configurations of the correct symmetry. A vertical excitation is the replacement of an occupied orbital by a virtual from its own stack and a singly ionic excitation is the double occupancy of a single virtual by means of a single vertical excitation along with one cross excitation. The reference space consisted of the spin-coupled configuration and the dominant configuration of each excited state. The dominant configuration for each excited state was found to correspond directly with the appropriate asymptotic separated-atom configuration. For the $^1\Sigma^+$ states, this procedure generated 65 VB structures, for the $^1\Pi$ states, 67 VB structures, for the $^3\Sigma^+$ states, just three VB structures, and for the $^3\Pi$ states, 24 VB structures. Further details on the

selection of virtual orbitals and on the construction of the SCVB expansions can be found in [10]. The basis set used here is somewhat smaller than those used in our previous studies of charge transfer processes, and the SCVB expansions are also much shorter. Our original aim was to investigate previous claims about the dominant role of rotational coupling, even at low energy. Nonetheless, in spite of the smaller scale of the present calculations than in our previous work, the overall agreement with experimental total cross sections turns out to be satisfactory. Further, we do not include endoergic channels, the lowest being to the $2p^2\ ^3P$, 1D , and 1S states, which are endoergic by 0.55, 1.0, and 4.5 eV/u. Those are expected to contribute only at the highest collision energies considered.

A comparison of our calculated asymptotic energy separations with experimental values is shown in Table I. The maximum deviation of the current results from the experimental energy separations is in the $2\ ^1\Sigma^+$ state, with an error of 0.25 eV. This is somewhat larger than the errors seen in much of our earlier work and is mostly a reflection of the choice of basis set. We cannot compare our asymptotic energy separations directly with those of Honvault *et al.* [6] as the values quoted in their paper were computed in separate atomic calculations on the B^{2+} and B^+ ions rather than from the full molecular calculation. The required degeneracies between asymptotic states of Σ^+ and Π symmetry are reproduced here to 0.02 eV or better. This high level of accuracy in the degeneracies is required for accurate values of the rotational coupling.

The resulting adiabatic potential energy curves and nonadiabatic coupling (both radial and rotational) were computed over the range $R = (1-20)a_0$. The adiabatic potential energy curves are illustrated in Fig. 1. The $2\ ^1\Sigma^+$ and $3\ ^1\Sigma^+$ adiabatic states have two avoided crossings: one at $12.21a_0$ with a very small energy separation $\Delta U(R_x)$ and another with a larger ΔU at $3.8a_0$. The third avoided crossing is between the $1\ ^1\Sigma^+$ and $2\ ^1\Sigma^+$ states at $4.48a_0$ and has a very large ΔU . There is only one avoided crossing between the two $^3\Sigma^+$ adiabatic potential curves, at $5.54a_0$ with ΔU of 2.767 eV. All the avoided crossing distances and ΔU values between the adiabatic potentials are listed in Table II. Hon-

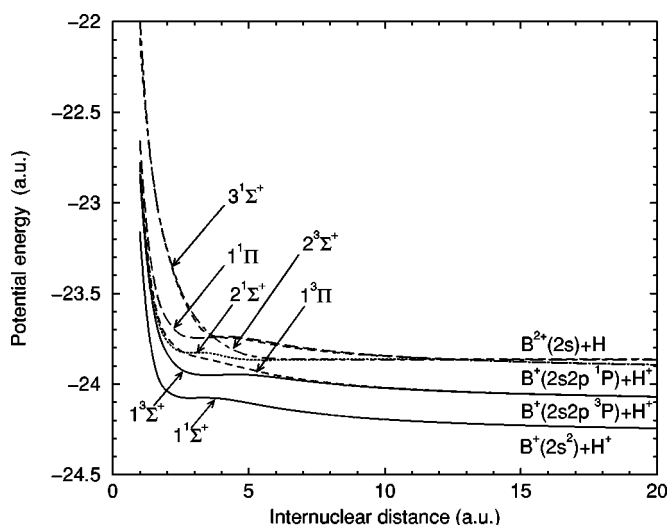


FIG. 1. The adiabatic potential energies for the BH^{2+} system as a function of internuclear distance R .

vault *et al.*'s [6] avoided crossing distances are also compared in Table II. For the $2^1\Sigma^+$ and $3^1\Sigma^+$ interaction, the larger distance at which Honvault *et al.*'s avoided crossing occurs indicates that their asymptotic energy separation between the two states is smaller than our value. Given that our energy separation is already smaller than the experimental value, this means that their value for the asymptotic energy separation is further removed from the experimental value than is ours. Honvault *et al.*'s [6] avoided crossings between the $1^1\Sigma^+$ and $2^1\Sigma^+$ states and between the $1^3\Sigma^+$ and $2^3\Sigma^+$ states seem to occur at much the same internuclear distances as our analogous avoided crossings, suggesting that the error in the values of their asymptotic energy separations between these channels is much the same as ours.

The computed radial couplings between the adiabatic states (matrix elements of $\partial/\partial R$) are illustrated in Fig. 2(a). The couplings were calculated using the central difference

TABLE II. Avoided crossing distances and energy separations for the adiabatic states of $B^{2+} + H$ (adiabatic labels).

Molecular states	R_x (units of a_0)	ΔU (eV)
$1^1\Sigma^+ - 2^1\Sigma^+$	4.48 ^a	6.342 ^a
	3.7 ^b	
	1.08 ^c	10.74 ^c
$2^1\Sigma^+ - 3^1\Sigma^+$	3.82 ^a	3.000 ^a
	2.7 ^b	
	2.53 ^c	13.86 ^c
$2^1\Sigma^+ - 3^1\Sigma^+$	12.21 ^a	0.008 ^a
	13 ^b	
	11.18 ^c	0.047 ^c
$1^3\Sigma^+ - 2^3\Sigma^+$	5.54 ^a	2.767 ^a
	5.4 ^b	
	3.69 ^c	9.24 ^c

^aThis work.

^bHonvault *et al.* [6].

^cEmpirical formula [20].

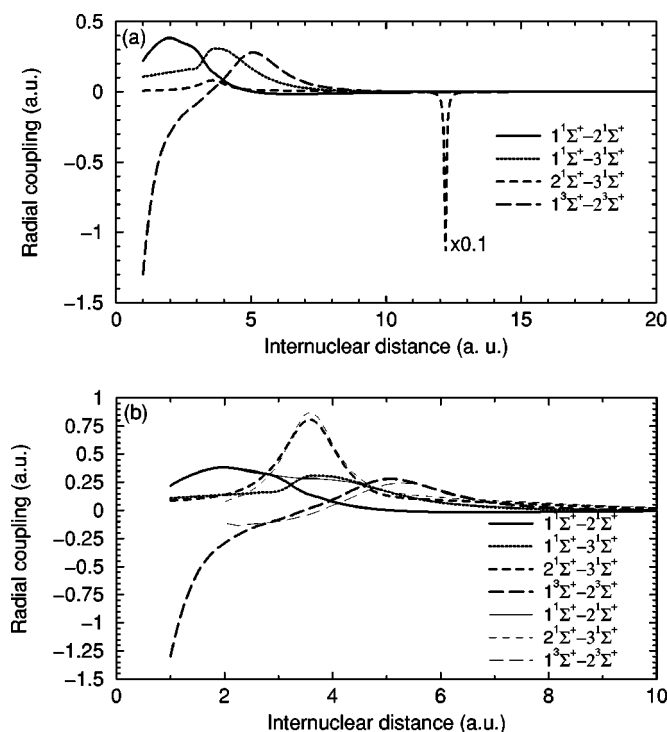


FIG. 2. Computed nonadiabatic radial coupling for the BH^{2+} system as a function of internuclear distance R . (a) Present calculations with the $2^1\Sigma^+ - 3^1\Sigma^+$ transition multiplied by 0.1. (b) Present calculations (thick lines) compared to those of Honvault *et al.* [6] (thin lines).

approximation with the electronic coordinate origin at the center of mass. The peaks corresponding to the avoided crossings are smooth, well defined, and centered on, or near, the positions of the avoided crossings. The couplings between nonadjacent states are much smaller than those between adjacent states and were found to have a negligible effect on the form of the p -diabatic potential energy matrices. As a consequence, they could be reset to zero for all internuclear separations. Honvault *et al.*'s [6] radial couplings are compared in Fig. 2(b). Except for the coupling between $1^1\Sigma^+$ and $2^1\Sigma^+$, the couplings of Honault *et al.* are similar to the current results.

Rotational couplings between the adiabatic states (matrix elements of the form $\langle \Psi_i | iL_y | \Psi_j \rangle$) have been computed using the Löwdin formula [12] for matrix elements between nonorthogonal determinants constructed from nonorthogonal spin orbitals. These couplings drive transitions between states of the same spin but of different spatial symmetry. The couplings between the $1^1\Sigma^+$ and $1^1\Pi$ states and between the $3^3\Sigma^+$ and $3^3\Pi$ states are shown in Fig. 3.

III. SCATTERING THEORY

The quantum-mechanical MOCC method, which we discuss only briefly here, has been described thoroughly in the literature [13,14]. It involves solving a coupled set of second-order differential equations. In the adiabatic representation, transitions between channels are driven by elements (radial \underline{A}^R and rotational \underline{A}^θ) of the vector potential

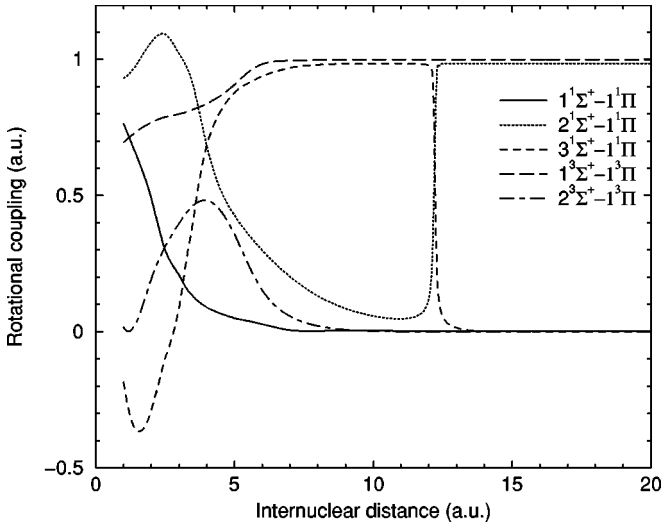


FIG. 3. Adiabatic rotational coupling for the BH^{2+} system as a function of internuclear distance R .

$\underline{A}(\vec{R})$, where \vec{R} is the internuclear distance vector. Since the adiabatic description contains first-order derivatives, it is numerically convenient to make a unitary transformation [8,13,15], which is affected by the radial portion of $\underline{A}(\vec{R})$, to the diabatic representation

$$\underline{U}(R) = \underline{W}(R)[\underline{V}(R) - \underline{P}(R)]\underline{W}^{-1}(R), \quad (2)$$

where $\underline{U}(R)$ is the diabatic potential matrix, $\underline{V}(R)$ is the diagonal adiabatic potential, $\underline{W}(R)$ is a unitary transformation matrix, and the elements of $\underline{P}(R)$ are¹

$$P_{mn} = \mp \frac{1}{\mu R^2} [(J \mp \lambda_m)(J \pm \lambda_m + 1)]^{1/2} A_{mn}^\theta \delta(\lambda_m, \lambda_n \mp 1) \quad (3)$$

(e.g., [17]) where μ is the reduced mass, J is the total angular momentum, and λ is the component of electronic angular momentum along the nuclear axis. The diagonal elements of the resulting p -diabatic potential energy matrices are displayed in Fig. 4, with the corresponding off-diagonal elements shown in Figs. 5 and 6. All of the elements of the p -diabatic potential energy matrices vary smoothly over the entire range of internuclear separations.

The electron capture cross section is given by

$$\sigma_{i \rightarrow j} = \frac{\pi}{k_i^2} \sum_J (2J+1) |S_J|_{i,j}^2, \quad (4)$$

where the S matrix is

$$\underline{S}_J = [\underline{I} + i\underline{K}_J]^{-1} [\underline{I} - i\underline{K}_J]. \quad (5)$$

The K matrix is obtained from the scattering amplitude after a partial-wave decomposition (e.g., Zygelman *et al.* [13])

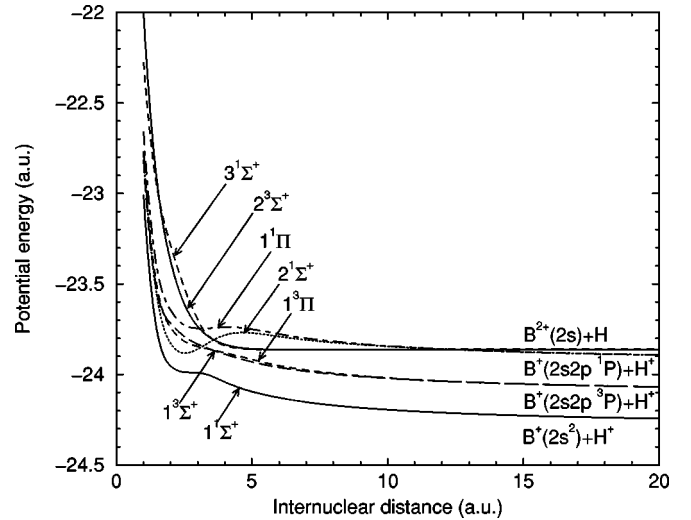


FIG. 4. The diabatic potential energies for the BH^{2+} system as a function of internuclear distance R .

and I is the identity matrix. Electron translation factors (ETFs; e.g., [14]) are not included. The influence of ETFs is expected to be important for $E > 1-5$ keV/u (e.g., [18,19]), which is near the upper limit of the calculated energy range.

IV. RESULTS AND DISCUSSION

The total and state-selective cross sections are calculated with and without rotational coupling. Without rotational coupling, the calculations are performed according to the symmetry $^1\Sigma^+$ (three-channel MOCC) and $^3\Sigma^+$ (two-channel MOCC). With rotational coupling, there are interactions between states with the same spin angular momentum, so that two calculations are performed, one for the singlet states $^1\Sigma^+$ and $^1\Pi$ (four-channel MOCC) and one for the triplet states $^3\Sigma^+$ and $^3\Pi$ (three-channel MOCC). Interactions between the singlet and triplet states via spin-orbit cou-

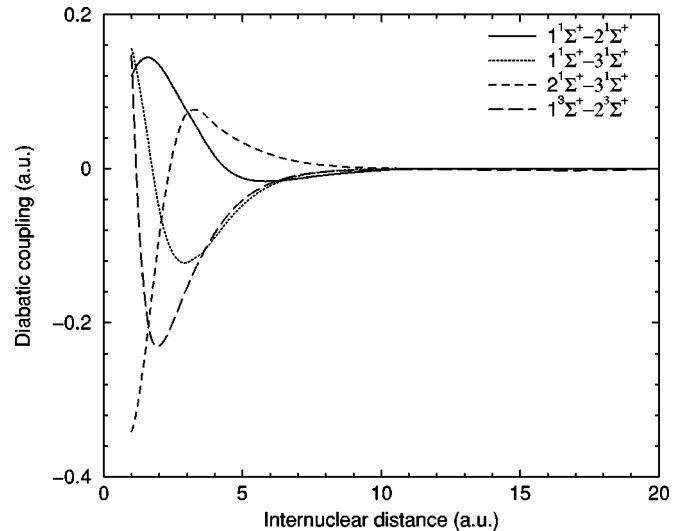


FIG. 5. Computed off-diagonal diabatic coupling for the BH^{2+} system as a function of internuclear distance R .

¹This equation corrects sign errors in Eq. (3) of [16].

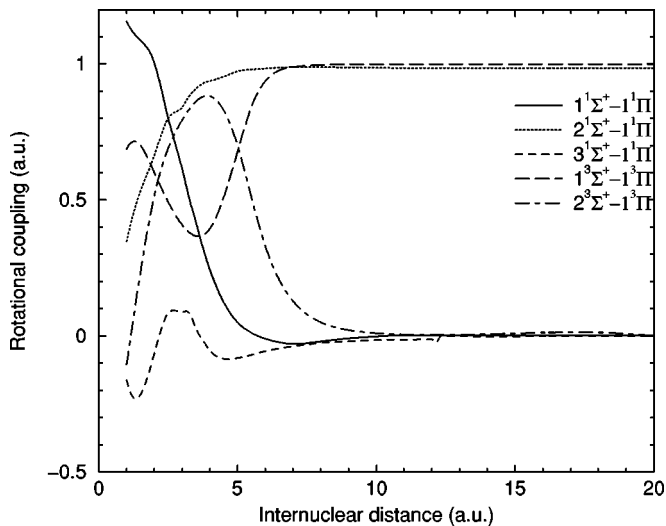


FIG. 6. Diabatic rotational coupling for the BH^{2+} system as a function of internuclear distance R .

pling are assumed to be small and are therefore neglected. The total and state-selective cross sections are obtained according to the statistical weight of the different symmetries, i.e., $\frac{1}{4}$ for singlets and $\frac{3}{4}$ for triplets. Convergence of the cross sections was ensured by including a sufficient number of partial waves J in Eq. (4). The maximum J increased with collision energy and depended somewhat on the symmetry. For example, for the singlets, 896 partial waves were needed for 10 eV/u, while 10 keV/u required 8960 partial waves. For the same collision energies, triplets converged after only 640 and 8320 partial waves, respectively.

A. Total cross sections

Figure 7 shows the total MOCC cross sections for the collisional energy range from 0.1 eV/u to 10 keV/u compared to the available calculations and measurements. At low collisional energy (< 5 eV/u), the cross sections display the typical Langevin $E^{-1/2}$ behavior. At about 10 eV/u, the total cross section reaches a local minimum and then increases to a local maximum at about 3 keV/u. When $E < 80$ eV/u, the differences between the current total MOCC cross sections with and without rotational coupling are small ($< 3\%$), demonstrating that rotational coupling is not important for low energy. With increasing energy, rotational coupling becomes more important. When $E > 400$ eV/u, the cross section including rotational coupling is 50%–80% larger than that without rotational coupling. In general, for total cross sections, rotational coupling is important in the higher-energy region. The cross sections were also calculated by the multichannel Landau-Zener (MCLZ) method using empirical parameters [20,21] and *ab initio* parameters in Table II. The MCLZ cross section with *ab initio* parameters has a similar energy dependence, but it is about half the MOCC result. On the other hand, use of empirical parameters in a MCLZ calculation results in a completely different behavior, which is a consequence of the different calculated ΔU as shown in Table II.

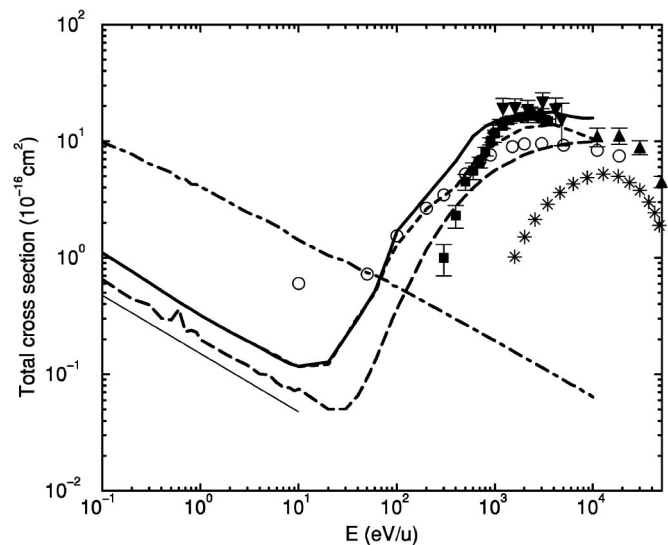


FIG. 7. Total electron capture cross sections for $B^{2+} + H$. Theory: MOCC calculation with rotational coupling (thick —), MOCC calculation without rotational coupling (thick - -), MCLZ with *ab initio* parameters (thick - · -), MCLZ with empirical parameters (thick - - -), Honvault *et al.* [6] (open circles), Crothers and Todd [5] (stars), and Dalgarno [23] (thin —). Experiment: Goffe *et al.* [2] (filled up triangles), McCullough *et al.* [1] (filled squares), Crandall *et al.* [3] (filled diamonds), and Gardner *et al.* [4] (filled down triangles).

Crothers and Todd's cross section [5] is much smaller than our result. This is because they considered only capture to $B^+(2s^2\ ^1S)$. Their cross section is in disagreement with the experimental data. Honvault *et al.*'s calculation [6] considered the $B^+(2s^2\ ^1S) + H^+$ and $B^+(2s2p\ ^1,3P) + H^+$ channels, and reproduced the experimental results much better than did the study of Crothers and Todd, but some disagreements remain. Our total cross sections show a markedly better agreement with the experimental cross sections than did the study of Honvault *et al.*, particularly in reproducing the peak in the total cross section. As we have considered all of the same entrance and exit channels as in the study of Honvault *et al.*, the differences are probably due to the molecular data adopted for the scattering calculations. For relatively low energies $E < 80$ eV/u, there is a significant difference between our total cross section and that of Honvault *et al.*, demonstrating a possible breakdown in the semiclassical approach in the low-energy range.

For $E < 1$ keV/u, the deviation between our calculations and McCullough *et al.*'s measurement [1] increases. In McCullough *et al.*'s experiment, a tungsten-tube furnace was used to provide a target of highly dissociated hydrogen, resulting in a target consisting of both H and H_2 . However, the SEC cross sections of B^{2+} with H and H_2 displayed different behaviors for $E < 1$ keV/u. The cross section for the H target decreases quickly with decreasing energy, while the cross section for the H_2 target increases. Even if only a small error exists in the measured H/ H_2 population ratio, subtraction of the H_2 cross section fraction may result in considerable uncertainty. This is consistent with ion-H merged-beam measurement which typically show difference with oven mea-

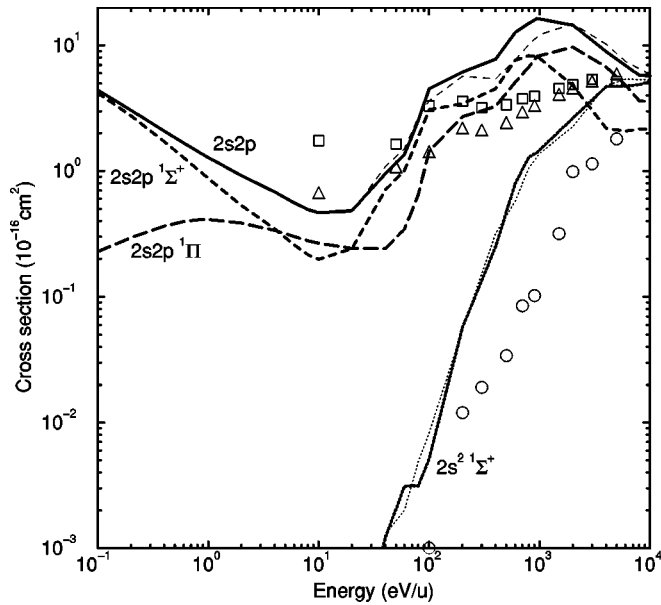


FIG. 8. State-selective cross sections for capture to singlet channels. MOCC with rotational coupling: $(2s^2)^1\Sigma^+$ (thick \cdots), $(2s2p)^1\Sigma^+$ (thick $- -$), $(2s2p)^1\Pi$ (thick $- -$), $(2s2p)^1\Sigma^+ + ^1\Pi$ (thick $-$). MOCC without rotational coupling: $(2s^2)^1\Sigma^+$ (thin \cdots), $(2s2p)^1\Sigma^+$ (thin $- -$). Honvault *et al.* [6]: $(2s^2)^1\Sigma^+$ (open squares), $(2s2p)^1\Sigma^+$ (open circles), $(2s2p)^1\Pi$ (open triangles). The statistical factor of 1/4 is not included for any of the presented data.

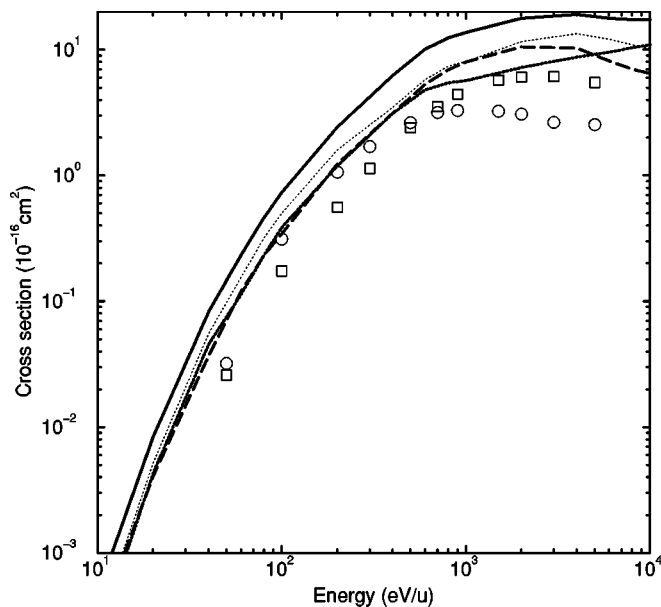


FIG. 9. State-selective cross sections for capture to triplet channels. MOCC with rotational coupling: $(2s2p)^3\Sigma^+$ (thick \cdots), $(2s2p)^3\Pi$ (thick $- -$), $(2s2p)^3\Sigma^+ + ^3\Pi$ (thick $-$). MOCC without rotational coupling: $(2s2p)^3\Sigma^+$ (thin \cdots). Honvault *et al.* [6]: $(2s2p)^3\Sigma^+$ (open circles), $(2s2p)^3\Pi$ (open squares). The statistical factor of 3/4 is not included for any of the presented data.

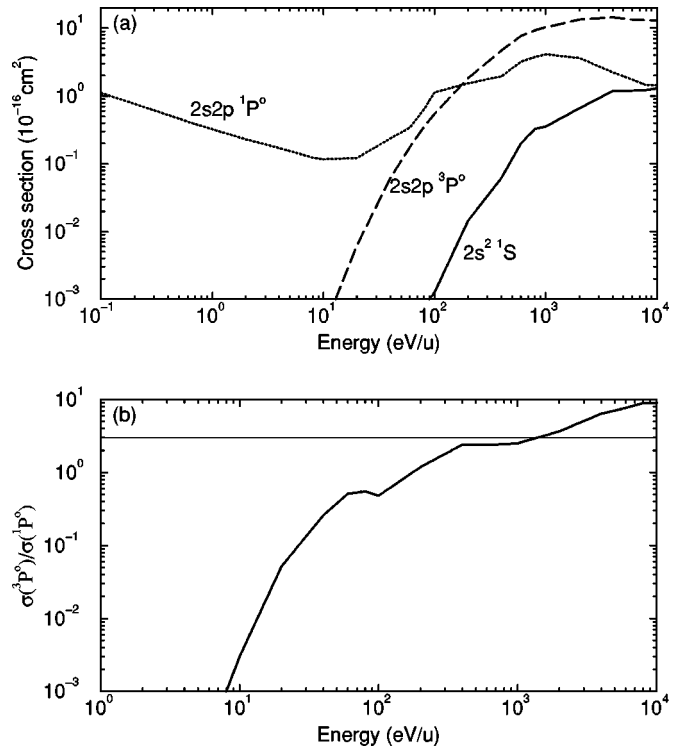


FIG. 10. (a) State-selective cross sections for capture to LS terms. MOCC with rotational coupling: $2s^2^1S$ (thick $-$), $2s2p^1P^o$ (thick \cdots), and $2s2p^3P^o$ (thick $- -$). (b) Ratio of cross sections for capture to $2s2p^3P^o$ and $2s2p^1P^o$. Present result (thick $-$); statistical argument (thin $-$).

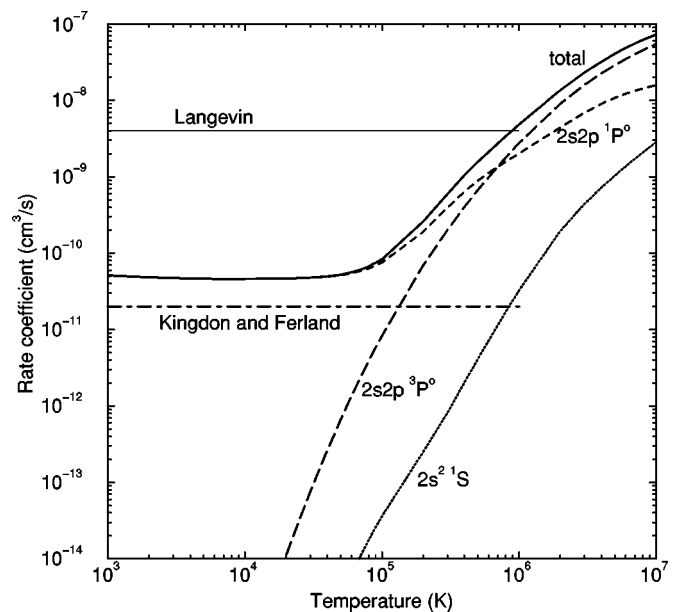


FIG. 11. Total and state-selective rate coefficients. MOCC total (thick $-$), $2s^2^1S$ (thick \cdots), $2s2p^1P^o$ (thick $- -$), $2s2p^3P^o$ (thick $-$). Kingdon and Ferland [24] (thick $- -$). Langevin formula (thin $-$).

TABLE III. MOCC SEC rate coefficients α (cm³ s⁻¹) for B²⁺ + H as a function of temperature T . Fitting parameters a_i (cm³ s⁻¹), b_i , and c_i (K) for the relation $\alpha(T) = \sum_i a_i (T/10\,000)^{b_i} \exp(-T/c_i)$ are given at the end of the table. Numbers in square brackets represent powers of ten.

T (K)	$2s\ ^1S$	$2p\ ^3P^0$	$2p\ ^1P^0$	Total
100			8.13[-11]	8.13[-11]
200			6.66[-11]	6.66[-11]
400			5.71[-11]	5.71[-11]
800			5.20[-11]	5.20[-11]
1000			5.09[-11]	5.09[-11]
2000			4.82[-11]	4.82[-11]
4000			4.65[-11]	4.65[-11]
10000			4.57[-11]	4.57[-11]
20000		1.13[-14]	4.64[-11]	4.64[-11]
40000	1.59[-15]	2.68[-13]	4.91[-11]	4.94[-11]
60000	6.33[-15]	1.36[-12]	5.47[-11]	5.60[-11]
80000	1.76[-14]	3.91[-12]	6.34[-11]	6.73[-11]
100000	3.65[-14]	8.39[-12]	7.52[-11]	8.36[-11]
200000	2.50[-13]	6.91[-11]	1.90[-10]	2.59[-10]
400000	2.03[-12]	4.02[-10]	6.36[-10]	1.04[-09]
600000	7.20[-12]	9.89[-10]	1.12[-09]	2.12[-09]
1000000	3.27[-11]	2.75[-09]	2.02[-09]	4.80[-09]
2000000	1.94[-10]	8.98[-09]	4.41[-09]	1.36[-08]
6000000	1.37[-09]	3.47[-08]	1.22[-08]	4.83[-08]
10000000	2.81[-09]	5.46[-08]	1.57[-08]	7.32[-08]
a_1	2.24[-17]	8.13[-16]	4.13[-11]	4.64[-11]
b_1	3.16	4.07	-1.11[-1]	-6.95[-2]
c_1	2.25[+6]	2.19[+5]	-1.67[+6]	1.28[+5]
a_2	1.60[-21]	4.34[-16]	1.05[-12]	1.08[-12]
b_2	4.26	3.24	1.70	1.86
c_2	6.59[+6]	2.50[+6]	3.73[+6]	5.49[+6]

surement at low energy [22]. A merged-beam measurement would be advantage to shed light on this discrepancy.

The calculations including rotational couplings lead to a modest improvement in the total cross section. This is particularly true for reproducing the peak height of the measurement. Because the ETF is not included in our calculations, the cross section for $E > 5$ keV/u may be not as reliable as that at lower energy, but we find that our cross sections for $E > 5$ keV/u can be connected smoothly with Goffe *et al.*'s measurement.

B. State-selective cross sections

State-selective cross sections for capture to the singlet channels are shown in Fig. 8 (without inclusion of the $\frac{1}{4}$ statistical factor). In the calculated energy range, capture to B⁺($2s2p\ ^1\Sigma^+, ^1\Pi$) dominates, while with increasing energy, capture to B⁺($2s^2\ ^1\Sigma^+$) becomes important. This is because capture to B⁺($2s^2\ ^1\Sigma^+$) occurs at a short avoided crossing distance ($4.48a_0$), while capture to B⁺($2s2p\ ^1\Sigma^+$) proceeds primarily through a long avoided crossing distance ($12.21a_0$) at low energy, with contributions from the short avoided crossing ($3.82a_0$) for higher energies. Figure 8 also shows MOCC results with and without rotational coupling.

Due to the strong rotational coupling between the B⁺($2s2p\ ^1\Sigma^+$) and B⁺($2s2p\ ^1\Pi$) channels, as shown in Figs. 3 and 6, these two channels are mixed so that the cross section for capture to B⁺($2s2p\ ^1\Pi$) is comparable to that for B⁺($2s2p\ ^1\Sigma^+$). Their summation at low energy ($E < 30$ eV/u) is similar to the cross section for capture to B⁺($2s2p\ ^1\Sigma^+$) without rotational coupling. With increasing energy, the B⁺($2s2p\ ^1\Sigma^+, ^1\Pi$) cross section becomes larger than the B⁺($2s2p\ ^1\Sigma^+$) cross section without rotational coupling. Therefore, rotational coupling is not the major capture process, as was originally implied by Honvault *et al.* [6], but it does provide some mixing between different symmetries.

The only state-selective results available for comparison are those due to the theoretical study of Honvault *et al.* [6], which are also plotted in Fig. 8. A quick inspection of the cross sections reveals a huge discrepancy between our B⁺($2s^2\ ^1\Sigma^+$) and B⁺($2s2p\ ^1\Sigma^+$) cross sections and those of Honvault *et al.* In fact, it appears that the cross sections have been mislabeled in the Honvault *et al.* paper: their cross section for capture to the B⁺($2s^2\ ^1\Sigma^+$) channel bears a remarkable similarity to our B⁺($2s2p\ ^1\Sigma^+$) cross section while their B⁺($2s2p\ ^1\Sigma^+$) cross section is also similar to

our $B^+(2s^2\ ^1\Sigma^+)$ cross section. Bacchus-Montabonel, one of the authors of the Honvault *et al.* paper, has been contacted and concurs that a mislabeling of the cross sections has taken place. With hindsight, it is obvious from the form of the potential energy curves that the cross sections have been labeled the wrong way round. We would expect the cross section for capture to the $B^+(2s2p\ ^1\Sigma^+)$ channel to be large at low collision energies and gradually decrease as the collision energy increases, because the avoided crossing between the adiabatic potential energy curves occurs at a relatively large internuclear separation. Conversely, we would expect the cross section for capture to the $B^+(2s^2\ ^1\Sigma^+)$ channel to be small at low collision energy and to increase as the collision energy increases, due to the avoided crossing occurring at a smaller internuclear separation. Apart from the labeling discrepancy, the cross sections of Honvault *et al.* seem to be similar to our results, although flatter. They do not reproduce the peaks in our $B^+(2s2p\ ^1\Sigma^+)$ and $B^+(2s2p\ ^1\Pi)$ cross sections seen at around 500 eV/u to 2000 eV/u.

State-selective cross sections for capture to triplet channels are shown in Fig. 9 compared to Honvault *et al.*'s results (without inclusion of the $\frac{3}{4}$ statistical factor). The cross sections are small at low energy as the triplets lack a long range avoided crossing. As for the singlet channels, rotational coupling mixes flux between the $B^+(2s2p\ ^3\Sigma^+)$ and $B^+(2s2p\ ^3\Pi)$ channels. Comparison with Honvault *et al.*'s results shows that our cross sections for capture to the $B^+(2s2p\ ^3\Sigma^+)$ and $B^+(2s2p\ ^3\Pi)$ channels are consistently larger over the entire range of collision energies for which comparable data are available.

In general, although capture to the $^1,^3\Pi$ channels via rotational coupling can be a significant process at certain collision energies, our calculations do not support the conclusion of Honvault *et al.* that capture driven by rotational coupling is crucial, particularly at low collision energies. Instead, the more typical case that radial coupling dominates the capture process holds for this collision system. Their conclusion was an unfortunate artifact of the error in cross section labeling.

State-selective cross sections for capture to different final B^+ states are shown in Fig. 10(a). They have been multiplied by the appropriate statistical weights. The ratio of cross sections for capture to $2s2p\ ^3P^o$ and $2s2p\ ^1P^o$ is plotted in Fig. 10(b). It is clearly seen that the usual statistical argument of a 3:1 ratio is violated at all energies except for $0.4 \leq E \leq 2$ keV/u.

C. Rate coefficients

Rate coefficients were computed by extending the cross section calculations to lower energy (1 meV/u) and averaging the cross sections over a Maxwellian velocity distribution. Total and state-selective rate coefficients are plotted in Fig. 11. Using the Landau-Zener approximation, Dalgarno [23] evaluated a constant total rate coefficient of 2×10^{-11} cm³/s for $T > 10^3$ K. This result was adopted by Kingdon and Ferland [24] for photoionized plasma models. For $T < 10^5$ K, the recommended rate coefficient is about 40% of our result. But for $T > 10^5$ K, our total rate coefficient increases very quickly, due to the contributions of the $B^+(2s2p\ ^3P^o)$ and $B^+(2s^2\ ^1S)$ channels. The rate coefficient from the Langevin formula is also plotted in Fig. 11, which is much larger than the current low-temperature result, demonstrating that the latter may not be reliable for low-charged ions which do not charge transfer through a resonant channel. Some numerical data and fits to these rate coefficients are presented in Table III. The fits do not deviate from the computed rate coefficients by more than 25% except for $2s2p\ ^3P^o$, where the discrepancy in the fit reaches 44% at high T .

V. SUMMARY

Quantum-mechanical MOCC calculations have been presented for electron capture following B^{2+} collisions with H over the collision energy range from 0.1 eV/u to 10 keV/u. The total and state-selective cross sections and rate coefficients are presented. Comparison with the existing experimental and theoretical data shows our total cross sections to be in better agreement with the measurements than previous calculations. Our calculations also show that rotational coupling becomes important with increasing collisional energy. For the total cross section, when $E > 400$ eV/u, rotational coupling increases the cross section by 50%–80%, which improves agreement with the experiments. From state-selective cross sections, it is shown that rotational coupling induces symmetry mixing, but that it is not a crucial process at low collisional energies as was mistakenly claimed by Honvault *et al.* [6].

ACKNOWLEDGMENTS

J.G.W. and P.C.S. acknowledge support from NASA Grant Nos. NAG5-9088 and NAG5-11453. We thank M. C. Bacchus-Montabonel and Charles Havener for helpful discussions and Bernard Zygelman for use of his MOCC code.

-
- [1] R.W. McCullough, W.L. Nutt, and H.B. Gilbody, *J. Phys. B* **12**, 4159 (1979).
 [2] T.V. Goffe, M.B. Shah, and H.B. Gilbody, *J. Phys. B* **12**, 3763 (1979).
 [3] D.H. Crandall, R.A. Phaneuf, and F.W. Meyer, *Phys. Rev. A* **19**, 504 (1979).
 [4] L.D. Gardner, J.E. Bayfield, P.M. Koch, I.A. Sellin, D.J. Pegg, R.S. Peterson, and D.H. Crandall, *Phys. Rev. A* **21**, 1397

(1980).

- [5] D.S.F. Crothers and N.R. Todd, *J. Phys. B* **13**, 547 (1980).
 [6] P. Honvault, M.C. Bacchus-Montabonel, and M. Druetta, *Mol. Phys.* **91**, 223 (1997).
 [7] B. Huron, J.P. Malrieu, and P. Rancurel, *J. Chem. Phys.* **58**, 5745 (1973).
 [8] D.L. Cooper, N.J. Clarke, P.C. Stancil, and B. Zygelman, *Adv. Quantum Chem.* **40**, 37 (2001).

- [9] M.F. Guest and P. Sherwood, GAMESS-UK User's Guide and Reference Manual, Revision B.0, Daresbury Laboratory, U.K., 1992 (unpublished).
- [10] A.R. Turner, Ph.D. thesis, University of Liverpool, 2002.
- [11] MOLPRO is a package of *ab initio* programs written by H-J. Werner and P.J. Knowles, with contributions from J. Almof, R.D. Amos, A. Berning, D.L. Cooper, M.J.O. Deegan, A.J. Dobbyn, F. Eckert, S.T. Elbert, C. Hampel, R. Lindh, A.W. Lloyd, W. Meyer, A. Nicklass, K. Peterson, R. Ptzer, A.J. Stone, P.R. Taylor, M.E. Mura, P. Pulay, M. Schutz, H. Stoll and T. Thorsteinsson.
- [12] P.O. Löwdin, Phys. Rev. **97**, 1474 (1955).
- [13] B. Zygelman, D.L. Cooper, M.J. Ford, A. Dalgarno, J. Gerratt, and M. Raimondi, Phys. Rev. A **46**, 3846 (1992).
- [14] M. Kimura and N.F. Lane, Adv. At. Mol. Opt. Phys. **26**, 79 (1990).
- [15] T.G. Heil, S.E. Butler, and A. Dalgarno, Phys. Rev. A **27**, 2365 (1983).
- [16] J.G. Wang, P.C. Stancil, A.R. Turner, and D.L. Cooper, Phys. Rev. A **67**, 012710 (2003).
- [17] B.H. Brandsen and M.R.C. McDowell, *Charge Exchange and the Theory of Ion-Atom Collisions* (Clarendon Press, Oxford, 1992).
- [18] R.K. Janev, L.P. Presnyakov, and V.P. Shevelko, *Physics of Highly Charged Ions* (Springer-Verlag, New York, 1985).
- [19] L.F. Errea, C. Harel, H. Jouin, L. Méndez, B. Pons, and A. Riera, J. Phys. B **27**, 3603 (1994).
- [20] S.E. Butler and A. Dalgarno, Astrophys. J. **241**, 838 (1980).
- [21] R.K. Janev, D.S. Belić, and B.H. Brandsen, Phys. Rev. A **28**, 1293 (1983).
- [22] M. Pieksma, M.E. Bannister, W. Wu, and C.C. Havener, Phys. Rev. A **55**, 3526 (1997).
- [23] A. Dalgarno, Proc. Phys. Soc. London **67**, 1010 (1954).
- [24] J.B. Kingdon and G.J. Ferland, Astrophys. J. **106**, 205 (1996).